

MAGNETIC ENERGY DISSIPATION IN FORCE-FREE JETS

ARNAB RAI CHOUDHURI

High Altitude Observatory, National Center for Atmospheric Research¹

AND

ARIEH KÖNIGL²

Department of Astronomy and Astrophysics, University of Chicago

Received 1985 December 19; accepted 1986 April 16

ABSTRACT

It is shown that a magnetic-pressure-dominated, supersonic jet which expands (or contracts) in response to variations in the confining external pressure can dissipate magnetic energy through field-line reconnection as it relaxes to a minimum-energy configuration. In order for a continuous dissipation to take place, the effective reconnection time must be a fraction $\epsilon \lesssim 1$ of the expansion time. For a force-free jet (with a magnetic field satisfying $\nabla \times \mathbf{B} = \mu \mathbf{B}$) in the axisymmetric ($m = 0$) minimum-energy state, the energy per unit length that is dissipated on the characteristic reconnection time scale (assuming conservation of magnetic helicity) is given by $(1/1152R^2)(\Psi/4\pi)^2\epsilon^2(\mu R)^6$ (where R is the jet radius and Ψ is the axial magnetic flux), to lowest order in ϵ and μR . On the basis of this result, it is concluded that magnetic energy dissipation could, in principle, power the observed synchrotron emission in extragalactic radio jets such as NGC 6251. However, just as in the case of analogous coronal heating models, this mechanism is only viable if the reconnection time is substantially shorter than the nominal resistive tearing time in the jet.

Subject headings: galaxies: jets — hydromagnetics — radiation mechanisms

I. INTRODUCTION

It has long been recognized that the synchrotron-radiating plasma in extragalactic radio jets must undergo continuous particle reacceleration in order to overcome the adiabatic and radiative losses sustained by the expanding flow (see, e.g., the review by Begelman, Blandford, and Rees 1984). The energy for the acceleration process has customarily been assumed to come from the bulk kinetic motion of the jet. Specifically, it has been suggested that a fraction of the bulk kinetic energy might be tapped through surface shear instabilities which could lead to a turbulent energy cascade in the jet and to the formation of internal shocks (e.g., Ferrari, Trussoni, and Zaninetti 1979; Smarr, Norman, and Winkler 1984). It has also been argued that the dissipation of the energy derived in this way could lead to efficient particle acceleration through the Fermi mechanism or by means of resonant interactions with MHD waves (e.g., Bicknell and Melrose 1982; Eilek and Henriksen 1984).

Recently, however, an alternative energy source for particle acceleration has been proposed in the context of the force-free-field model for magnetized supersonic jets (Königl and Choudhuri 1985; hereafter Paper I). According to this model, once a jet becomes magnetic-pressure dominated, it tends to settle down to that equilibrium field configuration which has the lowest magnetic energy for the given magnetic helicity. This unique configuration can be expressed as a superposition of the first two modes ($m = 0$ and $m = 1$) in the Chandrasekhar-Kendall representation of linear force-free fields (Taylor 1974). Any element of the jet which propagates through a region of varying external pressure has to undergo continuous field redistribution in order to satisfy the pressure-balance condition at the boundary while maintaining a minimum-energy configuration. It was suggested that this rearrangement process might be accompanied by field-line reconnection, and that the energy liberated in this fashion could then power the synchrotron emission from the jet.

The energy-dissipation scheme just described bears a strong analogy to certain recent proposals regarding the heating mechanism in the solar corona (Norman and Heyvaerts 1983; Heyvaerts and Priest 1984; Browning and Priest 1986). According to these models, the energy for the heating is derived from photospheric fluid motions which build up stresses within magnetic flux tubes that extend into the corona; some of this energy can then be released in the magnetically dominated region above the photosphere as the flux tubes relax to the lowest accessible energy state that is compatible with conservation of magnetic helicity. In much the same vein, one can envision the magnetic field lines in a jet being braided and twisted at the base of the flow (which is in fact, how they, acquire a nonvanishing helicity) and subsequently releasing the accumulated stresses through reconnection at large distances from the source. The main difference between these two scenarios lies in the fact that the field relaxation process in a jet is triggered by the changes in the external pressure which confines the super-Alfvénic flow, whereas in the solar case it is initiated by the footpoint motions of the quasistatic flux tubes. As a consequence of this, the evolution of a jet can be modeled as a steady state process in which the magnetic helicity per unit length remains constant along the flow (see Paper I), whereas the simplest footpoint motions considered in the coronal heating models generally involve a change in the magnetic helicity of the associated flux tubes. The basic principle underlying the energy dissipation mechanism remains, however, the same in both cases.

¹ The National Center for Atmospheric Research is sponsored by the National Science Foundation.

² Presidential Young Investigator.

Heyvaerts and Priest (1984) have investigated the conditions under which the field-redistribution process could give rise to magnetic energy dissipation. Although they have carried out this study in the context of their coronal heating model, their results are applicable also to the case of force-free jets. They found that the expected evolution depends essentially on the magnitude of one parameter, $\epsilon \equiv \tau_r/\tau_v$, the ratio of the characteristic field reconnection time to the characteristic dynamical time (where τ_v corresponds to the duration of a radial expansion or contraction in the case of a jet and to the photospheric footpoint transit time in the case of a solar flux tube). For $\epsilon \ll 1$ (the “instantaneous relaxation” limit), the magnetic energy dissipation is negligible since there is no buildup of magnetic stresses, and the field can maintain a linear force-free configuration at all times. This fact had already been noted in connection with certain plasma confinement schemes (see Bevir, Gimblett, and Miller 1985), and is given a general proof in Browning and Priest (1986) and Berger (1985). For $\epsilon > 1$, a buildup of a nonlinear force-free field configuration is predicted, with an eventual release of the stored magnetic stresses in an explosive, flare-like event (see Sturrock and Uchida 1981). Only for $\epsilon \lesssim 1$ is it possible for magnetic energy to be dissipated continuously at a nonnegligible rate.

In the original discussion of the field relaxation scenario in jets given in Paper I, the energy dissipation rate was calculated in the limit $\epsilon \rightarrow 0$, but an algebraic error led to a finite (instead of identically vanishing) result for the $m = 1$ mode (see Königl and Choudhuri 1986). Turner (1986) has recently given an explicit calculation of the dissipation rate in this limit, and concluded that no magnetic energy is available for powering the synchrotron radiation. In this paper we present a new derivation of the expected dissipation rate in the more interesting limit $\epsilon \lesssim 1$. In § II we formulate the problem and give an analytic derivation of the dissipation rate for the axisymmetric ($m = 0$) minimum-energy field configuration. In § III we discuss our result and conclude that the field relaxation process could be a viable mechanism for powering the synchrotron emission in extragalactic jets.

II. MAGNETIC ENERGY DISSIPATION FOR THE $m = 0$ MODE

In calculating the expected magnetic energy dissipation in a super-Alfvénic, force-free jet, we adopt the “mixing time” approach first employed by Heyvaerts and Priest (1984) in their coronal-heating model. In this approximation it is assumed that a cylindrical element of the jet, which initially has an $m = 0$ field configuration and a radius R_i , attains its final minimum-energy state at a radius R_f in two steps. In the first step, the element is deformed from R_i to R_f under ideal-MHD conditions, resulting in a *nonlinear* force-free field configuration. In the second step, that field configuration is allowed to relax to the *linear* ($m = 0$) force-free state corresponding to the new radius R_f , with the difference in energies being dissipated away. This process is assumed to occur on the reconnection time scale τ_r , which is shorter than the deformation time scale τ_v .

The adopted “mixing time” approximation is illustrated in Figure 1 with the help of phase-space diagrams. Figure 1a (Fig. 1b) depicts an expansion (contraction) of the jet from some initial value \tilde{V}_i of the volume per unit length to a final value \tilde{V}_f that occurs in response to a change in the confining pressure p_e from p_i to p_f . In the “instantaneous relaxation” limit, the jet remains in the $m = 0$ state (represented by the Taylor path ATB), and the $p_e d\tilde{V}$ work done by the external medium (corresponding to the area under ATB) is, as we have seen in Paper I, exactly equal to the change $\Delta\tilde{W}_{m=0}$ in the internal magnetic energy per unit length. For $\epsilon \lesssim 1$, we approximate the real path of the jet (represented schematically by ARB) with the two-legged trajectory ACB. In the first leg (AIC), the jet undergoes an ideal-MHD deformation to the final volume \tilde{V}_f , whereas in the second leg (CB) it relaxes to the $m = 0$ state corresponding to that volume. In the case of expansion (contraction), the $p_e d\tilde{V}$ work done on (by) the external medium along the path AIC (which is equal to the change $|\Delta\tilde{W}_{\text{ideal}}|$ in the magnitude of the internal magnetic energy per unit length during the ideal-MHD phase) is smaller (larger) than the corresponding work along the Taylor-relaxed path ATB (see the Appendix for an explicit demonstration of this fact). Hence, for both expansion and contraction, the energy difference $\Delta\tilde{W}_{\text{dis}} = \Delta\tilde{W}_{\text{ideal}} - \Delta\tilde{W}_{m=0}$ (corresponding to the area enclosed by ATBCIA) is a positive quantity, representing the magnetic energy available for dissipation.

In what follows, we first summarize the relevant features of the $m = 0$ field configuration presented in Paper I, and then calculate, in turn, $\Delta\tilde{W}_{\text{ideal}}$, $\Delta\tilde{W}_{m=0}$, and the expected dissipation rate corresponding to $\Delta\tilde{W}_{\text{dis}}$. An alternative derivation of $\Delta\tilde{W}_{\text{dis}}$, based on a direct application of the $p_e d\tilde{V}$ diagrams introduced in Figure 1, is given in the Appendix.

a) The Minimum-Energy Configuration

As discussed in Paper I, the minimum-energy equilibrium configuration corresponds to a locally linear force-free field, i.e., to a field satisfying $\nabla \times \mathbf{B} = \mu\mathbf{B}$, with μ locally a constant. As long as the product μR (where R is the radius of the locally cylindrical jet) is smaller than 3.11, the minimum-energy state is axisymmetric ($m = 0$ mode). The field components are then given (in cylindrical coordinates r, θ, z) by

$$B_r = 0, \quad B_\theta = B_0 J_1(\mu r), \quad B_z = B_0 J_0(\mu r), \quad (1)$$

where J_0 and J_1 are Bessel functions. The associated specific magnetic energy $\tilde{W}_{m=0}$ (energy per unit length) is

$$\tilde{W}_{m=0} = \left(\frac{\Psi}{4\pi}\right)^2 \frac{\mu R}{R^2} \left\{ \frac{\mu R [J_0^2(\mu R) + J_1^2(\mu R)] - J_0(\mu R)J_1(\mu R)}{J_1^2(\mu R)} \right\}, \quad (2)$$

where

$$\Psi = \frac{2\pi B_0 R^2}{\mu R} J_1(\mu R) \quad (3)$$

is the conserved axial magnetic flux. The other quantity besides Ψ which remains constant along the jet is the specific magnetic helicity \tilde{K} , given by

$$\tilde{K} = \left(\frac{\Psi}{4\pi}\right)^2 \frac{1}{R} \left\{ \frac{\mu R [J_0^2(\mu R) + J_1^2(\mu R)] - 2J_0(\mu R)J_1(\mu R)}{J_1^2(\mu R)} \right\}. \quad (4)$$

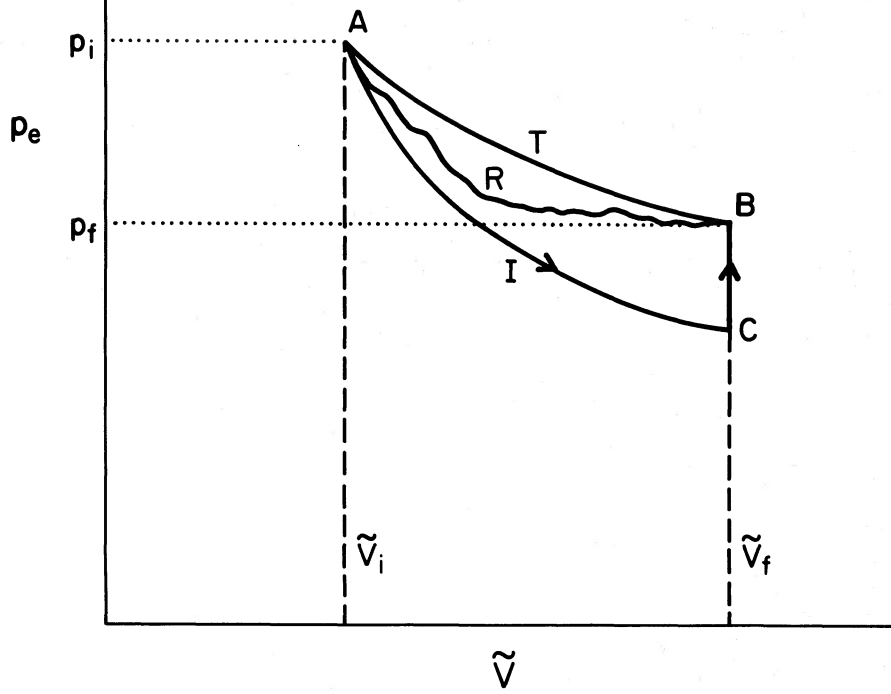


FIG. 1a

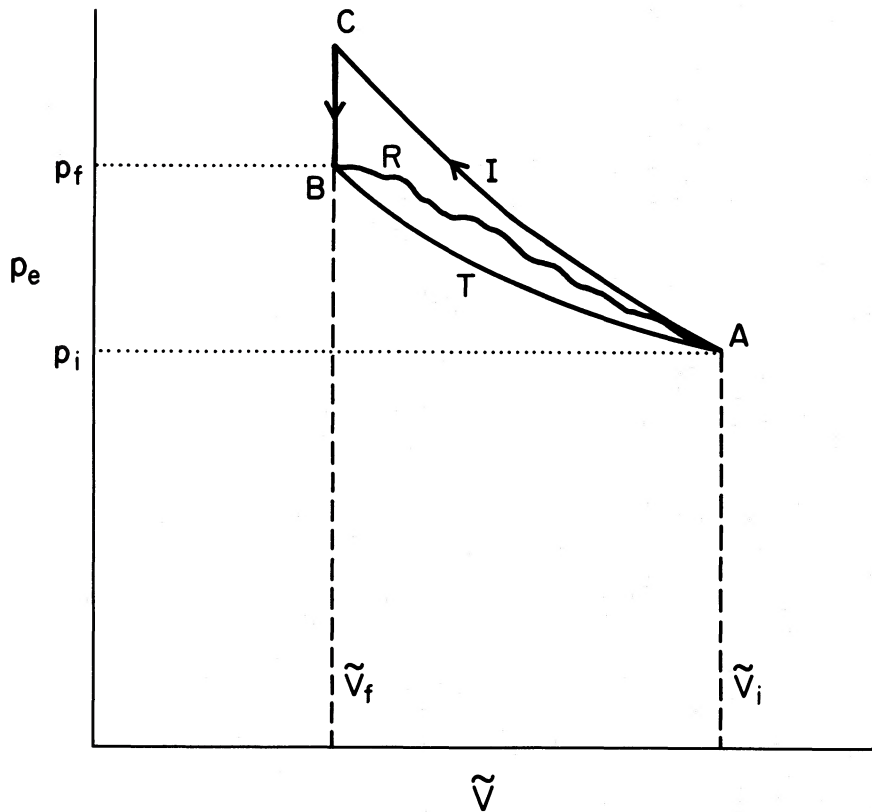


FIG. 1b

FIG. 1.—Schematic illustration of the “mixing time” approximation in the $p_e - \tilde{V}$ plane (where p_e is the confining external pressure and \tilde{V} is the volume per unit length of the jet). The diagrams in (a) and (b) correspond, respectively, to expansion and contraction of the jet from some initial minimum-energy configuration i to a final equilibrium state f . The segments labeled “T,” “I,” and “R” represent, respectively, the $m = 0$ Taylor state, the ideal-MHD configuration, and the expected trajectory of a real jet. The arrows indicate the path along the trajectory used in this approximation.

b) Calculation of $\Delta\tilde{W}_{\text{ideal}}$

The evolution of the field under an ideal-MHD deformation can be treated by the same method that has originally been developed to study the general properties of an isolated, twisted flux tube (see Parker 1979, Chap. 9). We describe the radial deformation of the jet by the mapping $r \rightarrow S(r)$, which must satisfy the boundary conditions $S(R_i) = R_f$ and $S(0) = 0$; this mapping may represent either an expansion or a contraction. The corresponding variation in the magnetic field structure is deduced from the requirement that both the axial and the azimuthal fluxes be conserved during the deformation; i.e.,

$$B_{z,i}(r)rd r = B_{z,f}[S(r)]S(r)dS, \quad (5a)$$

$$B_{\theta,i}(r)dr = B_{\theta,f}[S(r)]dS, \quad (5b)$$

where the subscripts i and f refer to the initial and final states, respectively. Since we are dealing with axisymmetric field configurations, it is convenient to introduce the *generating function* for force-free fields $F(r) \equiv B_{\theta}^2(r) + B_z^2(r)$, from which the individual field components can be derived by using

$$B_{\theta}^2 = -\frac{1}{2}r \frac{dF}{dr}, \quad B_z^2 = F + \frac{1}{2}r \frac{dF}{dr} \quad (6)$$

(e.g., Parker 1979). By combining equations (5) and (6), we obtain the following pair of coupled first-order differential equations for $S(r)$ and $F_f(r)$:

$$S(r) \left(\frac{dF_f}{dr} \right)_{r=S(r)} \left[\frac{dS(r)}{dr} \right]^2 = r \frac{dF_i(r)}{dr}, \quad (7a)$$

$$\left\{ F_f[S(r)] + \frac{1}{2} S(r) \left(\frac{dF_f}{dr} \right)_{r=S(r)} \right\} S^2(r) \left[\frac{dS(r)}{dr} \right]^2 = \left[F_i(r) + \frac{1}{2} r \frac{dF_i(r)}{dr} \right] r^2, \quad (7b)$$

where the initial generating function is given by

$$F_i(r) = \frac{4}{R_i^4} \left(\frac{\Psi}{4\pi} \right)^2 \frac{(\mu_i R_i)^2}{J_1^2(\mu_i R_i)} [J_0^2(\mu_i r) + J_1^2(\mu_i r)] \quad (8)$$

(see eqs. [1] and [3]).

According to the basic assumption underlying this calculation, the elemental step under consideration occurs on a time scale $\tau_r = |\epsilon| \tau_v$, during which the radius of the jet changes by an amount $\sim \tau_r (R/\tau_v) = \epsilon R$. Since we only consider the case $|\epsilon| \leq 1$, we shall treat ϵ as a small expansion parameter; in this formulation ϵ can be either positive or negative, depending on whether R increases or decreases. We thus write

$$S(r) = r + \epsilon T(r) + \epsilon^2 U(r) + O(\epsilon^3), \quad (9a)$$

$$F_f(r) = F_i(r) + \epsilon M(r) + \epsilon^2 N(r) + O(\epsilon^3). \quad (9b)$$

The reason for expanding $F_f(r)$ to second order in ϵ is that the lowest order terms which appear in the expression for $\Delta\tilde{W}_{\text{dis}}$ (eq. [17] below) are $O(\epsilon^2)$. Physically, this is because we are considering perturbations of linear force-free equilibria which represent extremum (i.e., minimum) energy states (see Browning and Priest 1986 for a formal proof). Another way of understanding this fact is to note that $\Delta\tilde{W}_{\text{dis}}$ must be a nonnegative quantity regardless of whether the jet expands ($\epsilon > 0$) or contracts ($\epsilon < 0$), so that it cannot scale linearly with ϵ . It is, however, unnecessary to include the $O(\epsilon^2)$ terms in the expression for $S(r)$ (eq. [9a]) when calculating $\Delta\tilde{W}_{\text{dis}}$ to that same order in ϵ (see discussion in Browning and Priest 1986); nevertheless, we retain the function $U(r)$ in our solution for the sake of self-consistency.

We now substitute equation (9) into equation (7), expand to $O(\epsilon^2)$, and solve for the functions T , U , M , and N . In order to obtain a solution in closed form, we perform a series expansion of the function $Y(x) \equiv J_0^2(x) + J_1^2(x)$ in the expression for $F_i(r)$ (eq. [8]) in terms of the parameter $x \equiv \mu_i r$, which gives

$$Y(x) = 1 - \frac{1}{4}x^2 + \frac{1}{32}x^4 - \frac{5}{2304}x^6 + O(x^8). \quad (10)$$

This expansion is plotted in Figure 2 together with the exact expression for $Y(x)$. As can be seen from this figure, the truncated series provides an excellent approximation to the original function for small values of x , with the first perceptible deviation occurring only around $x = 1.6$. Substituting this approximation to $F_i(r)$ into equation (7), we obtain, after some algebra,

$$S = r \left\{ 1 + \epsilon \left[1 + \frac{1}{8}x^2 + \frac{1}{192}x^4 - \frac{1}{4608}x^6 + O(x^8) \right] + \epsilon^2 \left[\frac{3}{16}x^2 + \frac{1}{48}x^4 - \frac{1}{3072}x^6 + O(x^8) \right] + O(\epsilon^3) \right\}, \quad (11a)$$

$$\begin{aligned} \Delta F \equiv F_f - F_i &= \frac{16}{R_i^4} \left(\frac{\Psi}{4\pi} \right)^2 \left(1 + \frac{1}{4}X_i^2 + \frac{7}{192}X_i^4 + \frac{19}{4608}X_i^6 \right) \\ &\times \left\{ -\epsilon \left[4 - x^2 + \frac{1}{16}x^4 + \frac{1}{288}x^6 + O(x^8) \right] + \epsilon^2 \left[10 - \frac{5}{2}x^2 - \frac{1}{32}x^4 + \frac{1}{64}x^6 + O(x^8) \right] + O(\epsilon^3) \right\}, \quad (11b) \end{aligned}$$

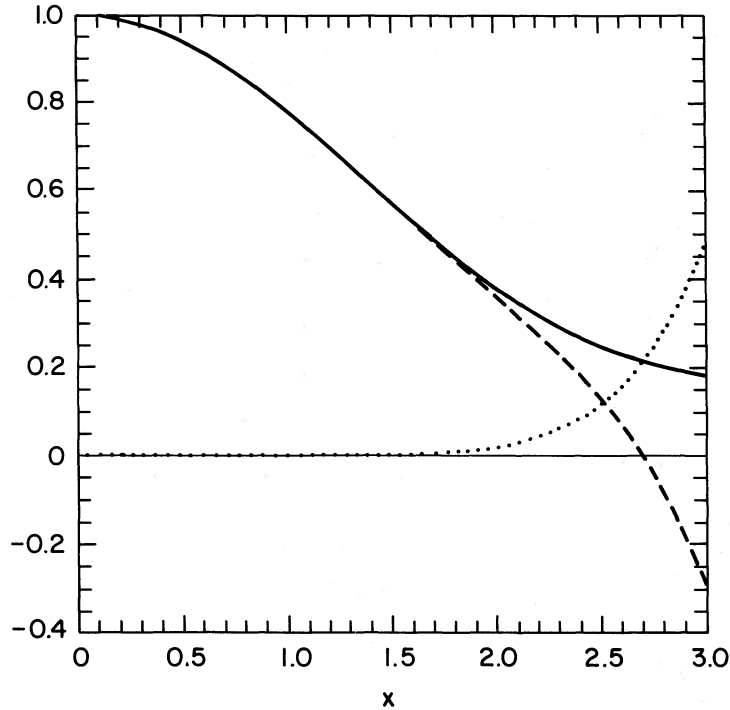


FIG. 2.—The function $Y(x) \equiv J_0^2(x) + J_1^2(x)$ (solid curve), which represents the generating function for the $m = 0$ mode. Also shown are the series expansion of this function to sixth order in x (dashed curve) and the difference between the exact and the approximate representations (dotted curve).

where the terms in $X_i \equiv \mu_i R_i$ represent the expansion of $X_i^2/J_1^2(X_i)$ in equation (8). The change in the specific magnetic energy associated with this ideal deformation is given by

$$\Delta \tilde{W}_{\text{ideal}} = \frac{1}{4} \left(\int_0^{R_f} \Delta F r dr + \int_{R_i}^{R_f} F_i r dr \right).$$

Using equations (8), (10), and (11), together with the boundary condition $S(R_i) = R_f$, we find

$$\Delta \tilde{W}_{\text{ideal}} = \frac{2}{R_i^2} \left(\frac{\Psi}{4\pi} \right)^2 \left\{ -\epsilon \left[2 + \frac{1}{4} X_i^2 + \frac{1}{48} X_i^4 + \frac{5}{2304} X_i^6 + O(X_i^8) \right] + \epsilon^2 \left[3 + \frac{3}{8} X_i^2 + \frac{1}{32} X_i^4 + \frac{1}{512} X_i^6 + O(X_i^8) \right] + O(\epsilon^3) \right\}. \quad (12)$$

c) Calculation of $\Delta \tilde{W}_{m=0}$

The change in the specific magnetic energy of the $m = 0$ field configuration between the initial and the final states can be obtained from equation (2). We again use equation (11a) to calculate $R_f = S(R_i)$. To evaluate μ_f , we employ the assumed constancy of the specific magnetic helicity \tilde{K} during the deformation. Expanding equation (4) in powers of μR , we get

$$\tilde{K} = \left(\frac{\Psi}{4\pi} \right)^2 \frac{\mu}{2} \left[1 + \frac{1}{2} (\mu R)^2 + \frac{1}{128} (\mu R)^4 + O(\mu^6 R^6) \right], \quad (13)$$

from which μ_f is found by iteration:

$$\mu_f = \mu_i \left\{ 1 - \epsilon \left[\frac{1}{6} X_i^2 + \frac{1}{96} X_i^4 + O(X_i^6) \right] - \epsilon^2 \left[\frac{1}{12} X_i^2 - \frac{1}{192} X_i^4 + O(X_i^6) \right] + O(\epsilon^3) \right\}. \quad (14)$$

Substituting into the expanded form of equation (2),

$$\tilde{W}_{m=0} = \frac{2}{R^2} \left(\frac{\Psi}{4\pi} \right)^2 \left[1 + \frac{1}{8} (\mu R)^2 + \frac{1}{64} (\mu R)^4 + \frac{5}{3072} (\mu R)^6 + O(\mu^8 R^8) \right], \quad (15)$$

we obtain

$$\Delta \tilde{W}_{m=0} = \frac{2}{R_i^2} \left(\frac{\Psi}{4\pi} \right)^2 \left\{ -\epsilon \left[2 + \frac{1}{4} X_i^2 + \frac{1}{48} X_i^4 + \frac{5}{2304} X_i^6 + O(X_i^8) \right] + \epsilon^2 \left[3 + \frac{3}{8} X_i^2 + \frac{1}{32} X_i^4 + \frac{7}{4608} X_i^6 + O(X_i^8) \right] + O(\epsilon^3) \right\}. \quad (16)$$

d) *The Energy Dissipation Rate*

The specific magnetic energy which is dissipated in the characteristic “reconnection time” can now be found by subtracting equation (16) from equation (12). To lowest order in ϵ and X_i , it is given by

$$\Delta \tilde{W}_{\text{dis}} = \frac{1}{1152R_i^2} \left(\frac{\Psi}{4\pi} \right)^2 \epsilon^2 X_i^6 = \frac{B_{0,i}^2 R_i^2}{18432} \epsilon^2 X_i^6, \quad (17)$$

where the last equality follows from equation (3). As anticipated (see § IIb), this expression is quadratic in ϵ . It is noteworthy that all powers of X_i lower than the sixth cancel out. In view of the comparison presented in Figure 2, we expect this expression to be fairly accurate even for X_i of order unity. Furthermore, since the next higher order term in ϵ can be written simply by replacing ϵ^2 in equation (17) with ϵ^3 (see eq. [A7] in the Appendix), this equation should provide a good estimate of the dissipated energy so long as $|\epsilon|$ is not too close to 1.

To estimate the specific dissipation rate \tilde{P}_m , we divide $\Delta \tilde{W}_{\text{dis}}$ by the nominal relaxation time τ_r . For a collimated jet moving with speed v in the z -direction, τ_r can be approximated by $\epsilon R_i/v(dR/dz)_{R=R_i}$. Hence

$$\tilde{P}_m = \frac{\epsilon(\mu R)^6}{18432} B_0^2 v R \frac{dR}{dz}, \quad (18)$$

where the subscript i has now been dropped. Equation (18) provides a direct illustration of the fact that the dissipated power vanishes in the limit $\epsilon \rightarrow 0$ (see § I). The coefficient $\epsilon(\mu R)^6/18432$ in this equation represents the “dissipation efficiency” of the $m = 0$ field configuration, and its derivation completes the calculation that we have set out to perform in this section.

III. DISCUSSION

In order to assess the astrophysical implications of the result derived in the preceding section, we evaluate equation (18) for the parameters appropriate to the inner region of the extended radio jet NGC 6251. (The application of the force-free equilibrium model to this source has been considered in detail in Paper I.) Substituting $B_0 = 2 \times 10^{-5}$ G, $v = 8 \times 10^8$ cm s $^{-1}$, $R = 3 \times 10^{21}$ cm, and $dR/dz = 0.05$ (see Perley, Bridle, and Willis 1984), we obtain $\tilde{P}_m = 2.6 \times 10^{15} \epsilon(\mu R)^6$ ergs s $^{-1}$ cm $^{-1}$. For $\epsilon = 1$ and $\mu R = 2$ (which are roughly the maximum permissible values for which eq. [8] remains applicable), we get a specific dissipation rate $\sim 2 \times 10^{17}$ ergs s $^{-1}$ cm $^{-1}$, which is comparable to the mean radio luminosity per unit length measured in this region. Although the radio luminosity provides only a lower bound to the total dissipated power, we note that the adopted values of v and B are also only lower limits to the actual magnitudes of these parameters in the jet. Furthermore, although the choice $\epsilon = 1$ was designed to optimize our estimate, even a lower value of ϵ could be more than compensated for by the strong dependence of \tilde{P}_m on μR . In fact, in view of the apparent nonaxisymmetric field configuration in the jet (which in this model indicates the presence of the $m = 1$ mode), we expect that the actual value of μR in the region under consideration is 3.11 (see § IIa). Even though our estimate of \tilde{P}_m does not apply in that regime (in particular, the evolution of a nonaxisymmetric field configuration cannot be described by the simple generating-function method adopted in § II), it is not unreasonable to expect that the dissipation rate continues to grow as μR increases and the field becomes progressively more sheared. We thus conclude that magnetic energy dissipation accompanying the field relaxation in a source like NGC 6251 could, in principle, power the observed synchrotron emission from the jet. We emphasize, in response to a question raised by Turner (1986), that the final field configuration envisioned in the present scheme is precisely the one that was applied in Paper I to the modeling of the various nonaxisymmetric radio features in NGC 6251. In this connection, we specifically distinguish between the protracted (but *complete*) relaxation process invoked in our calculation and the incomplete relaxation process considered, for example, by Turner and Christiansen (1981), for which the existence of a nonaxisymmetric, minimum-energy final state has not been explicitly demonstrated. We also note that the expected strong dependence of \tilde{P}_m on μR may be relevant to the interpretation of the radio “gaps” observed near the origins of certain extended sources, since μR should increase with distance along the jet if its initial value is less than 3.11 (see Fig. 3 in Paper I; an alternative interpretation of the “gaps” is suggested in the next paragraph).

The major uncertainty in our model is associated with the value of ϵ , which depends on the magnitude of the characteristic reconnection time τ_r . This time scale may be expected to be of the order of the growth time τ_i of the resistive tearing-mode instability. In the linear regime of this instability, $\tau_i \sim (\tau_d \tau_A)^{1/2}$, where τ_d is the Ohmic dissipation time and τ_A is the Alfvén crossing time (both corresponding to the width of the jet). Under astrophysical circumstances (in either jets or the solar corona), the value of τ_i calculated in this way is very much larger than the relevant dynamical time scale (whereas the proposed relaxation scheme requires $\tau_r \lesssim \tau_v$). In addressing this problem, Heyvaerts and Priest (1984) and Browning and Priest (1986) suggested that, in the nonlinear regime, reconnection could proceed on a time scale as short as $\sim 10\tau_A$. If this is indeed the minimum value of τ_r in a jet, then the condition $\epsilon \lesssim 1$ implies that the Alfvén Mach number of the flow cannot exceed $\sim (10dR/dz)^{-1}$. Laboratory plasma confinement experiments (e.g., Wojtowicz *et al.* 1985; Wright *et al.* 1985) could conceivably help to identify the relevant relaxation time scale. We note that the $m = 0$ field configuration becomes (linearly) unstable to resistive tearing only after μR reaches 3.11 (Gibson and Whiteman 1968). Thus, if this instability dominates the field reconnection process in the jet, then the presence of “gaps” could perhaps be attributed to the fact that the outflow first becomes strongly dissipative at the turn-on points of the $m = 1$ mode.

Another general question pertaining to our estimate concerns the efficiency with which the dissipated magnetic energy can be converted into synchrotron radiation. In the shear-dissipation schemes that had previously been suggested for powering the synchrotron emission (see § I), it was often argued that particle acceleration (leading to nonthermal radiation) provides the main damping mechanism for the induced turbulence (e.g., Bicknell and Melrose 1982; Eilek and Henriksen 1984). The same dissipation processes (including Fermi acceleration and resonant wave-particle interactions) are likely to operate also in the case of a relaxing

force-free jet, since the formation of minimum-energy states is apparently directly related to the development of MHD turbulence (e.g., Montgomery, Turner, and Vahala 1978). Furthermore, in the magnetic-dissipation model, particle acceleration could also be effected by DC electric fields in the field-line reconnection sites associated with the tearing-mode instability. (This mechanism is, in fact, thought to play an important role in the acceleration of fast particles in solar flares; e.g., Heyvaerts 1981.) It is thus conceivable that a significant fraction of the magnetic energy released in the jet during the field relaxation process could be transformed into nonthermal radiation.

We are grateful to Mitch Berger for a critical reading of the manuscript. A. K. thanks the Institute for Theoretical Physics, University of California, Santa Barbara, for hospitality during part of this work. A. R. C. began this work as a research assistant at the University of Chicago, whereas the final part of the work was done while he was a visiting scientist at the National Center for Atmospheric Research. This research was supported in part by NSF grants AST 84-51727 and AST 85-03093, and NASA grant NGL 14-001-001 at Chicago.

APPENDIX

AN ALTERNATIVE DERIVATION OF $\Delta\tilde{W}_{\text{dis}}$

In this Appendix, the quantity $\Delta\tilde{W}_{\text{dis}}$ (eq. [17]) is derived directly from a consideration of the work done by the jet in pushing against the confining external medium, without separately calculating $\Delta\tilde{W}_{\text{ideal}}$ and $\Delta\tilde{W}_{m=0}$ as in § II. For this purpose, we make use of the $p_e d\tilde{V}$ diagrams introduced in Figure 1. The present calculation, in turn, serves to justify the relative positions of the various phase-space trajectories depicted in this figure.

As we pointed out at the beginning of § II, the change in the internal magnetic energy per unit length during both an ideal-MHD deformation (labeled by "I" in Fig. 1) and a minimum-energy deformation (labeled by "T" in that figure) is exactly equal to the $p_e d\tilde{V}$ work done by the external medium under conditions of pressure equilibrium at the jet boundary. For this reason, one can express the energy difference $\Delta\tilde{W}_{\text{dis}} \equiv \Delta\tilde{W}_{\text{ideal}} - \Delta\tilde{W}_{m=0}$ in the form

$$\Delta\tilde{W}_{\text{dis}} = \int_{\mathcal{P}_i}^{\mathcal{P}_f} [p_{m=0}(\tilde{V}) - p_{\text{ideal}}(\tilde{V})] d\tilde{V} = 2\pi \int_{R_i}^{R_f} [p_{m=0}(R) - p_{\text{ideal}}(R)] R dR, \quad (\text{A1})$$

where $p_{m=0}$ and p_{ideal} are, respectively, the boundary pressure values along the ATB and AIC trajectories in Figure 1, and where the other symbols have the same meaning as in § II. Note that equation (A1) is valid for both an expansion (Fig. 1a) and a contraction (Fig. 1b) of the jet.

The values of R between R_i and R_f can be conveniently labeled by introducing a parameter ϵ' which is zero at R_i and ϵ at R_f , where ϵ is the expansion parameter that appears in equation (9). Treating ϵ' as the new independent variable in equation (A1), we can rewrite it as

$$\Delta\tilde{W}_{\text{dis}} = 2\pi \int_0^\epsilon [p_{m=0}(\epsilon') - p_{\text{ideal}}(\epsilon')] R(\epsilon') \frac{dR}{d\epsilon'} d\epsilon', \quad (\text{A2})$$

where, by equation (11a),

$$R(\epsilon') = R_i \left\{ 1 + \epsilon' \left[1 + \frac{1}{8} X_i^2 + \frac{1}{192} X_i^4 - \frac{1}{4608} X_i^6 + O(X_i^8) \right] + \epsilon'^2 \left[\frac{3}{16} X_i^2 + \frac{1}{48} X_i^4 - \frac{1}{3072} X_i^6 + O(X_i^8) \right] + O(\epsilon'^3) \right\}. \quad (\text{A3})$$

The functions $p_{\text{ideal}}(\epsilon')$ and $p_{m=0}(\epsilon')$ are obtained by noting that they are equal to $1/8\pi$ times the corresponding generating functions, F_f and F_i , evaluated at the boundary. Using equations (8), (10), and (11b) (with r replaced by $R[\epsilon']$) as well as equation (A3), we get

$$p_{\text{ideal}}(\epsilon') = \frac{2}{\pi R_i^4} \left(\frac{\Psi}{4\pi} \right)^2 \left\{ 1 + \frac{1}{192} X_i^2 + \frac{1}{1536} X_i^6 + O(X_i^8) + \epsilon' \left[-4 - \frac{1}{2} X_i^2 - \frac{1}{48} X_i^4 - \frac{1}{576} X_i^6 + O(X_i^8) \right] + \epsilon'^2 \left[10 + \frac{7}{4} X_i^2 + \frac{17}{96} X_i^4 + \frac{5}{576} X_i^6 + O(X_i^8) \right] + O(\epsilon'^3) \right\}. \quad (\text{A4})$$

Similarly, using equations (8) and (10) (with μ_i replaced by $\mu_f[\epsilon']$ and with R_i and r replaced by $R[\epsilon']$), and substituting for $\mu_f(\epsilon')$ from equation (14) (in which ϵ is replaced by ϵ') and for $R(\epsilon')$ from equation (A3), we obtain

$$p_{m=0}(\epsilon') = \frac{2}{\pi R_i^4} \left(\frac{\Psi}{4\pi} \right)^2 \left\{ 1 + \frac{1}{192} X_i^2 + \frac{1}{1536} X_i^6 + O(X_i^8) + \epsilon' \left[-4 - \frac{1}{2} X_i^2 - \frac{1}{48} X_i^4 - \frac{1}{768} X_i^6 + O(X_i^8) \right] + \epsilon'^2 \left[10 + \frac{7}{4} X_i^2 + \frac{17}{96} X_i^4 + \frac{41}{4608} X_i^6 + O(X_i^8) \right] + O(\epsilon'^3) \right\}. \quad (\text{A5})$$

Equations (A4) and (A5) can be combined to give

$$p_{m=0}(\epsilon') - p_{\text{ideal}}(\epsilon') = \frac{\epsilon'}{1152\pi R_i^4} \left(\frac{\Psi}{4\pi} \right)^2 \left[\left(1 + \frac{1}{2} \epsilon' \right) X_i^6 + O(X_i^8) + O(\epsilon' X_i^8) \right] + O(\epsilon'^3), \quad (\text{A6})$$

which shows that $p_{m=0}$ exceeds p_{ideal} in the case of expansion ($\epsilon' > 0$), and vice versa for contraction ($\epsilon' < 0$). Equation (A6) thus confirms that the relative positions of the ATB and AIC trajectories in Figures 1a and 1b are as drawn. It also substantiates the claim, made in § II, that the work done by an expanding jet in pushing against the external medium is smaller along the path AIC than along ATB, with the opposite conclusion applying to the work done on a contracting jet along these trajectories.

Using equations (A3) and (A6), we can perform the integral in equation (A2) to obtain

$$\Delta\tilde{W}_{dis} = \frac{1}{1152R_i^2} \left(\frac{\Psi}{4\pi}\right)^2 \epsilon^2 [(1 + \epsilon)X_i^6 + O(X_i^8) + O(\epsilon X_i^8)] + O(\epsilon^4). \quad (A7)$$

Equation (A7) agrees with equation (17) to $O(\epsilon^2)$ and also gives explicitly the ϵ^3 correction term. The reason why this term could be self-consistently derived with the present method is that both $R(\epsilon')$ (eq. [A3]) and $p_{m=0}(\epsilon') - p_{ideal}(\epsilon')$ (eq. [A6]), which appear as factors in the integrand of equation (A2), have been expanded to $O(\epsilon'^2)$, so the integral (over ϵ') of their product is manifestly accurate to $O(\epsilon^3)$. (The factor $dR(\epsilon')/d\epsilon'$ in the integrand of eq. [A2] is $O(1)$ if only $O(X_i^6)$ terms are retained.) By contrast, the fact that $\Delta\tilde{W}_{dis}$ can be calculated to $O(\epsilon^3)$ even though the basic variables are expanded only to $O(\epsilon^2)$ is not readily recognized when the method of § II is used.

REFERENCES

- Begelman, M. C., Blandford, R. D., and Rees, M. J. 1984, *Rev. Mod. Phys.*, **56**, 255.
 Berger, M. A. 1985, *Ap. J. Suppl.*, **59**, 433.
 Bevir, M. K., Gimblett, C. G., and Miller, G. 1985, *Phys. Fluids*, **28**, 1826.
 Bicknell, G. V., and Melrose, D. 1982, *Ap. J.*, **262**, 511.
 Browning, P. K., and Priest, E. R. 1986, *Astr. Ap.*, **159**, 129.
 Eilek, J. A., and Henriksen, R. N. 1984, *Ap. J.*, **277**, 820.
 Ferrari, A., Trussoni, E., and Zaninetti, L. 1979, *Astr. Ap.*, **79**, 190.
 Gibson, R. D., and Whiteman, K. J. 1968, *Plasma Phys.*, **10**, 1101.
 Heyvaerts, J. 1981, in *Solar Flare Magnetohydrodynamics*, ed. E. R. Priest (New York: Gordon & Breach), p. 429.
 Heyvaerts, J., and Priest, E. R. 1984, *Astr. Ap.*, **137**, 63.
 Königl, A., and Choudhuri, A. R. 1985, *Ap. J.*, **289**, 173 (Paper I).
 ———. 1986, *Ap. J.*, **305**, 954.
 Montgomery, D., Turner, L., and Vahala, G. 1978, *Phys. Fluids*, **21**, 757.
 Norman, C. A., and Heyvaerts, J. 1983, *Astr. Ap.*, **124**, L1.
 Parker, E. N. 1979, *Cosmical Magnetic Fields* (Oxford: Clarendon Press).
 Perley, R. A., Bridle, A. H., and Willis, A. G. 1984, *Ap. J. Suppl.*, **54**, 291.
 Smarr, L. L., Norman, M. L., and Winkler, K.-H. A. 1984, *Physica*, **12D**, 83.
 Sturrock, P. A., and Uchida, Y. 1981, *Ap. J.*, **246**, 331.
 Taylor, J. B. 1974, *Phys. Rev. Letters*, **33**, 1139.
 Turner, L. 1986, *Ap. J.*, **305**, 668.
 Turner, L., and Christiansen, J. P. 1981, *Phys. Fluids*, **24**, 893.
 Wojtowicz, S. S., Jensen, T. H., Ikezi, H., Jackson, G. L., and Newman, D. E. 1985, *Bull. Am. Phys. Soc.*, **30**, 1449.
 Wright, B. L., Fernandez, J. C., Jarboe, T. R., and Platts, D. A. 1985, *Bull. Am. Phys. Soc.*, **30**, 1454.

ARNAB RAI CHOUDHURI: High Altitude Observatory, National Center for Atmospheric Research, P.O. Box 3000, Boulder, CO 80307

ARIEH KÖNIGL: Astronomy and Astrophysics Center, University of Chicago, 5640 S. Ellis Avenue, Chicago, IL 60637